

Accepted Manuscript

Title: Chlorpyrifos Degradation via Photoreactive TiO₂
Nanoparticles: Assessing the Impact of a Multi-Component
Degradation Scenario

Authors: Jeffrey Farner Budarz, Ellen M. Cooper, Courtney
Gardner, Emina Hodzic, P. Lee Ferguson, Claudia K. Gunsch,
Mark R. Wiesner



PII: S0304-3894(17)30918-4
DOI: <https://doi.org/10.1016/j.jhazmat.2017.12.028>
Reference: HAZMAT 19060

To appear in: *Journal of Hazardous Materials*

Received date: 9-6-2017
Revised date: 8-12-2017
Accepted date: 9-12-2017

Please cite this article as: Farner Budarz J, Cooper EM, Gardner C, Hodzic E, Ferguson PL, Gunsch CK, Wiesner MR, Chlorpyrifos Degradation via Photoreactive TiO₂ Nanoparticles: Assessing the Impact of a Multi-Component Degradation Scenario, *Journal of Hazardous Materials* (2010), <https://doi.org/10.1016/j.jhazmat.2017.12.028>

This is a PDF file of an unedited manuscript that has been accepted for publication. As a service to our customers we are providing this early version of the manuscript. The manuscript will undergo copyediting, typesetting, and review of the resulting proof before it is published in its final form. Please note that during the production process errors may be discovered which could affect the content, and all legal disclaimers that apply to the journal pertain.

Chlorpyrifos Degradation via Photoreactive TiO₂ Nanoparticles: Assessing the Impact of a Multi-Component Degradation Scenario

Jeffrey Farner Budarz^a, Ellen M. Cooper^b, Courtney Gardner^a, Emina Hodzic^b, P. Lee
Ferguson^a, Claudia K. Gunsch^a, Mark R. Wiesner^{a,c}

^a Department of Civil and Environmental Engineering, Pratt School of Engineering, Duke University, Durham, North Carolina, 27708, USA

^b Duke University Nicholas School of the Environment, Durham, North Carolina 27708, USA

^c Corresponding author phone: 919-660-5292; fax: 919-660-5219; e-mail: wiesner@duke.edu

Highlights

- Chlorpyrifos adsorption to TiO₂ NPs is not observed to any appreciable extent.
- Loss of chlorpyrifos is predominantly due to photocatalytic degradation.
- Association with TiO₂ results in greater hydroxyl radical delivery.
- Bacterial inactivation is unaffected by system complexity due to NP proximity.
- Simplified systems may overestimate photocatalytic efficiency for some targets.

ABSTRACT

High concentrations of pesticides enter surface waters following agricultural application, raising environmental and human health concerns. The use of photoreactive nanoparticles has shown promise for contaminant degradation and surface water remediation. However, it remains uncertain how the complexity of natural waters will impact the photodegradation process. Here, we investigate the photoreactivity of titanium dioxide nanoparticles, the capability to degrade the pesticide chlorpyrifos, and the effect of and impact on bacteria during the photodegradation process. Loss of chlorpyrifos in solution resulted solely from photocatalytic oxidation, with 80% degradation observed after 24h in our reactor, either in the presence or absence of bacteria. Degradation of chlorpyrifos to chlorpyrifos oxon and 3,5,6-trichloro-2-pyridinol was observed via LC/MS-MS and effectively modeled for the given reactor conditions. Bacterial inactivation occurred over 60 minutes and was not impacted by the presence of chlorpyrifos. The relative affinity of bacteria and chlorpyrifos for the

nanoparticle surface decreased the amount of Reactive Oxygen Species (ROS) detected in the bulk by up to 94%, suggesting that ROS measurements in simplified systems may overestimate the reactivity of photoreactive nanoparticles in complex environments.

Keywords: Titanium Dioxide, Nanoparticles, Photoreactivity, Chlorpyrifos, Bacterial

Inactivation

1. INTRODUCTION

Chlorpyrifos (CPF) is an organophosphate pesticide used for agricultural applications such as cotton, corn, and fruit trees, as well as at high concentrations in wood for anti-termite applications [1-4]. As a result, CPF has been frequently observed in agricultural runoff and urban streams [5-8]. Both CPF and its primary oxidation products, chlorpyrifos oxon (CPF Oxon) and 3,5,6-trichloropyridinol (TCP), are of considerable environmental concern due to high fish and aquatic invertebrate toxicity, as well as known human health concerns [9-13].

CPF was designed to be susceptible to base catalysis, with a half-life in water on the order of days, though studies of adsorbed CPF indicate that the half-life can range from hundreds of days to years [4, 14-17]. Gebremariam et al., in reviewing the literature, observed a significant spread in the extent of CPF adsorption to various soil types, though a strong linear relationship was seen with soil organic content, implicating the hydrophobic binding sites present on organic matter [4]. Rose et al. observed that the loss of CPF from a water column in the presence of natural colloidal matter occurred more rapidly than other common pesticides studied [18]. However, rainfall has been shown to be sufficient for CPF-particle resuspension, which may lead to increased bioavailability and transport [4, 14, 19].

Photocatalytic degradation holds promise for dealing with aquatic contamination [20-26]. Nanoscale TiO₂ is widely studied for remediation applications due to its photochemical properties and ability to provide a steady, continual source of reactive oxygen species (ROS) [27, 28]. CPF degradation experiments employing TiO₂ as the radical generator often employ high concentrations of the catalyst (0.1 – 12 g L⁻¹) in an effort to maximize radical production and minimize treatment time, with CPF loss often occurring within hours [27, 29, 30]. What remains unclear, however, is to what extent the observed loss of CPF from the solution is due to sorption versus degradation. CPF's affinity for soils may not translate to TiO₂, as sorption of CPF increases with organic content [4]. Furthermore, little absorption has been seen for similar pesticides when employing metal oxide nanoparticles (NPs) [17, 31-33]. This question is of particular importance in light of the high surface area of NPs and their potential to act as pollutant transport vectors should incomplete degradation occur [34-36].

Additionally, many types of bacteria have been observed to degrade CPF, including *Bacillus* and *Acinetobacter* strains isolated from groundwater sources, either using the pesticide as the sole carbon source or cometabolically [2, 16, 37-41]. Biodegradation may be an appealing approach to CPF remediation, though longer residence times are necessary compared to chemical or external remediation techniques [42].

High levels of pollutants may also be toxic to bacteria and hinder bioremediation efforts. Toxicity studies of CPF and its degradation products have shown that there is an impact on both individual species and entire bacterial communities [43-45]. When concentrations of CPF are high, pretreatment of contaminated water may improve remediation efforts. TCP was calculated to be 2.5 times less toxic than CPF for a model bacterium, indicating that pretreatment achieving even partial degradation of a pollutant may facilitate bioremediation efforts [5].

A mixed or sequential approach combining nanoremediation with a biological component may be a more efficient and cost effective treatment method. Within this context, our understanding of the microbial response in a UV/TiO₂ remediation system is currently lacking, with the concern existing that any nanoremediation strategy will harm the natural bacterial community. ROS production by the UV/TiO₂ system will possibly be of more consequence than the pollutant [43, 46-50].

In this paper we investigate the process of CPF loss in water utilizing UV/TiO₂, both in the presence and absence of bacteria. We hypothesize that CPF loss in the system is primarily due to photocatalytic degradation, rather than sorption. Additionally, we test the hypothesis that the UV/TiO₂ process will inactivate bacteria to a greater extent than will CPF or its degradation products, reducing the likelihood of bioremediation. In contrast to studies that have been primarily designed to maximize degradation of CPF, the reactor conditions employed here were selected to highlight the interactions between TiO₂, CPF, and bacteria. Furthermore, this work highlights the importance that the water constituents have on bulk TiO₂ reactivity.

2. MATERIALS AND METHODS

2.1. TiO₂ Suspension and Characterization

Experiments were performed with P25 Aeroxide TiO₂ (Evonik Industries, Essen, Germany), a nanoparticulate TiO₂ consisting of fused rutile and anatase crystalline phases at roughly a 20/80% ratio, respectively. TiO₂ NPs were suspended in a Minimal Davis media (MD) designed to stabilize the particles, buffer the pH at 7.5, and maintain bacterial viability, as described by Lyon et al. [51]. Briefly, MD media consists of 0.45 g L⁻¹ K₂HPO₄, 0.25 g L⁻¹ sodium citrate, 0.5 g L⁻¹ (NH₄)₂SO₄, and 0.05 g L⁻¹ MgSO₄•7H₂O. The lowered phosphate concentration reduces quenching of ROS by the media. Suspensions were produced via probe sonication (Q700, QSonica, Newton, CT, USA) run in pulse mode (12 s on, 3 s off) for 6 minutes total following the protocol by Taurozzi et al. [52] and subsequently characterized in terms of aggregate size, surface charge, and ROS production. Dynamic light scattering (ALV-CGS3, ALV-GMBH, Langen, Germany) and transmission electron microscopy (TEM) (Tecnai G² Twin, FEI, Hillsboro, OR, USA) were performed to determine aggregate size, while electrophoretic mobility measurements (EPM) were taken with the Zetasizer Nano ZS (Malvern, Bedford, MA, USA).

2.2. UV Irradiation and Photoreactivity

CPF was exposed to TiO₂ both in the presence and absence of UV light to investigate the relative effects of sorption and degradation. UV irradiation was performed with two 15 W fluorescent bulbs (Philips TLD 15W BLB, Koninklijke Philips, Eindhoven, The Netherlands) having a peak emission at 365 ± 15 nm. Samples were placed in batch reactors and continually stirred using glass stir bars via magnetic stir plates with UV irradiation from above. Reactors contained a total of 10 mL, with an illuminated surface area of 25.5 cm². For UV experiments involving CPF, reactors were covered with glass petri dishes to minimize loss due to volatilization. The temperature inside the reaction chamber was kept at 23°C. The net irradiance at the suspension surface was 2.3 mW cm⁻² for bacterial inactivation experiments and 2.0 mW cm⁻² for CPF degradation tests, measured by a UVX radiometer with UV-A filter (UVP, inc., Upland, CA, USA). TiO₂ reactivity was also characterized with and without CPF to explore how CPF affinity for the TiO₂ surface relative to other species in water impacts degradation efficacy.

ROS production was measured via probe compounds and quenching agents. For hydroxyl radical (•OH) measurements, terephthalic acid (TA) (98% Sigma-Aldrich, St. Louis, MO, USA) and N-acetyl-L-cysteine (N-AC) (Sigma-Aldrich) were used as probe and quencher, respectively, where •OH generation was measured as the increase in fluorescent units (FSU) resulting from the oxidation of 125 µM TA to 2-hydroxyterephthalic acid (2-HTA) (ex. 315nm / em. 425nm). Superoxide (O₂•-) was detected as the increase in FSU at 586nm (excitation at 510nm) resulting from the transformation of 50 µM dihydroethidium (DHE) in solution to 2-hydroxyethidium (2-HE) (Invitrogen, Thermo Fisher Scientific, Waltham, MA, USA). Superoxide dismutase (SOD) (Sigma-Aldrich) was used as the O₂•- quenching agent.

Dark controls were run to test CPF adsorption to the NP surface, CPF was spiked into MD media containing TiO₂ nanoparticles at 0 mg L⁻¹ (control), 20 mg L⁻¹, and 40 mg L⁻¹ and allowed to mix in the dark. Reaction vials were covered tightly in aluminum foil and were periodically sampled over 24 h. All concentrations were run in triplicate.

2.3. Bacterial Cultures

Gram positive *Bacillus subtilis* strain 168 ATCC 23857 and Gram negative *Acinetobacter baumannii* ATCC 49466 (ATCC, Manassas, VA, USA) were chosen as model bacteria based upon their environmental relevance, documented ability to biodegrade CPF, and cell membrane structure. Pure cultures of *A. baumannii* and *B. subtilis* were grown overnight at 37°C in tryptic soy broth. Cells were pelleted at 8,000 rpm for 10 min and washed thrice with MD. Cells were then resuspended in MD to a final concentration of 10⁹ cells mL⁻¹. Two mL aliquots of the bacterial suspension were added to each batch reactor.

To determine if CPF degradation products impact bacteria, we exposed cultures of *B. subtilis* and *A. baumannii* to CPF, CPF Oxon, and TCP, individually. Toxicity of the products arising from photocatalytic degradation was investigated by exposing CPF for 60 min to UV/TiO₂. Suspensions of *B. subtilis* and *A. baumannii* were then dosed with the resulting combination of CPF, TiO₂ nanoparticles, and CPF degradation products present in the system. Additionally, bacteria were exposed to the UV/TiO₂ to evaluate the biological impact of remediation attempts.

Samples taken from the batch reactors for inactivation measurements were serially diluted to obtain a final concentration of 10^3 CFU mL⁻¹. One hundred μ L of the final dilution was then spread onto tryptic soy agar plates in triplicate and allowed to grow overnight at 37°C. The resulting colonies were then counted, and ROS and CPF toxicity was calculated as log inactivation relative to time zero.

TEM images of Bacteria and TiO₂ NPs were obtained by depositing samples on lacey carbon grids. These were fixed with 2.5% glutaraldehyde, and sequentially dehydrated and washed with graded ethanol and 1x phosphate-buffered saline (PBS), respectively.

2.4. Chlorpyrifos

Chlorpyrifos (99.5%, Chem Service, West Chester, PA, USA) stocks were made in methanol at 1.5 g L⁻¹, which were diluted in MD to working stocks at 1.5 mg L⁻¹. For all experiments, CPF was spiked into samples at 375 μ g L⁻¹. Stocks of CPF degradation products CPF Oxon (analytical standard, AccuStandard, New Haven, CT, USA) and 3,5,6-trichloro-2-pyridinol (analytical standard, Sigma-Aldrich) suspensions were similarly prepared.

2.5. Sample Preparation and Analysis

At each sampling point, a 0.2 mL aliquot was transferred to a 1 mL tapered base glass reaction vial (Kimble Chase, Vineland, NJ) along with 10 μ L formic acid to aggregate TiO₂ nanoparticles. Samples were centrifuged for 2 min at 9,000 rpm and the supernatant transferred to an LC/MS vial and spiked with 100 μ L 1 μ g/mL each deuterated chlorpyrifos and ¹³C₆-3,5,6-trichloro-2-pyridinol (Cambridge Isotopes, Cambridge, MA) and diluted to a final volume of 0.5 mL in 20% acetonitrile (ACN, Honeywell Burdick & Jackson, Muskegon, MI) to match initial LC mobile phase conditions (described below). Residue in the reaction vial was extracted three times with 300 μ L ACN and 10 μ L formic acid via sonication for 5 min followed by centrifugation (described above). Extracts were combined, concentrated to 100 μ L under N₂, spiked and diluted as described above. Glass pipettes were used at all times (e.g. when sampling individual time points and transferring aliquots during extractions).

CPF and its degradation products were analyzed by LC/MS-MS using electrospray ionization in positive (CPF and CPF Oxon) and negative (TCP) modes with a Thermo Accela UPLC system and Thermo TSQ Vantage mass spectrometer (Thermo Scientific). Separation was achieved on a Synergi Polar RP column (50 mm x 2.0 mm, 2.5 μ m particle size, Phenomenex, San Jose, CA) and a 400 μ L min⁻¹ gradient of 5 mM formic acid (A) and 5 mM formic acid (B) in ACN with the following conditions: 0-0.2 min 70:30 A:B to 1:99 A:B at 3-4 min with return to initial conditions at 5 min and re-equilibration for 4 min. Source conditions included spray voltages +3.5 kV/-2.5 kV, vaporizer temperature 350°C, capillary temperature 375°C, sheath gas 45 psi and auxiliary gas 10 psi. Target analytes and internal standards were monitored using the transitions described in Table SI-1. Method detection limits were 1.51 \pm 0.49 ng/mL (CPF), 0.13 \pm 0.02 ng/mL (CPF Oxon), and 3.61 \pm 1.84 ng/mL (TCP), and spike recoveries for all analytes were >93%. Further validation criteria for LC/MS-MS analysis are described in Table SI-2.

2.6. CAKE Software Package

The computer-assisted kinetic evaluation (CAKE) v3.1 software package, developed by Tessella (Abingdon, UK) was used to determine degradation rates and pathways (details in SI-6). Single first order (SFO) fitting was employed for CPF degradation as well as CPF Oxon and TCP formation. CPF degradation was assumed to proceed to CPF Oxon, TCP, or an undetermined sink. CPF Oxon degradation was assumed to proceed to TCP or an undetermined sink. TCP degradation was assumed to proceed to an undetermined sink. Using this kinetic schema, the software then fits the data to the proposed pathways, returning rate constants and relative weights of each pathway.

3. RESULTS

3.1. TiO₂ Characterization and Reactivity

Sonicated P25 in MD produced a narrow distribution of aggregates with an average radius of 94.7 nm and a polydispersity index (PDI) of 0.06 as determined by DLS, and confirmed with TEM. The resulting suspensions were stable, with no aggregation observed over 6 h via time resolved DLS (Figure SI-1). TiO₂ aggregates were negatively charged at pH 7.5, with an electrophoretic mobility of $-3.79 \pm 0.11 \times 10^{-8} \text{ m}^2 \text{ V}^{-1} \text{ s}^{-1}$ (ζ potential of $-48.4 \pm 1.4 \text{ mV}$), and the presence of the media decreased the isoelectric point from the point of zero charge of bare P25 (pH ~6.5) to a pH of approximately 1.5 (Data in SI1). Both $\bullet\text{OH}$ and $\text{O}_2\bullet^-$ generation was observed, with production rapidly reaching steady state. The use of N-AC and SOD effectively quenched $\bullet\text{OH}$ and $\text{O}_2\bullet^-$ production, respectively (Figure SI-2).

3.2. CPF Interactions with the TiO₂ surface

No significant loss of CPF from solution is observed under dark conditions in the presence of either 20 or 40 ppm TiO₂ NPs (Figure 1). Concentrations of CPF extracted from the TiO₂ surface were minimal, and no trend was observed either with increased time or TiO₂ concentration. Additionally, these small losses occur in the control samples as well as in the presence of TiO₂ and likely represent sorption of CPF to the glass walls of the sampler vials after the aliquot has been taken. When combining the supernatant and extract concentrations, CPF recovery compared to $t = 0$ for both dark and control samples ranged from 89.5 to 101.5%.

Figure 1 - Supernatant CPF concentrations versus time as a function of TiO₂ concentration (0, 20, 40 mg L⁻¹ dark and 20 mg L⁻¹ UV). UV irradiance at the suspension surface was 2.0 mW cm⁻².

3.3. CPF UV/TiO₂ Degradation

Suspensions of CPF and TiO₂ were exposed to UV light to initiate photodegradation. Approximately 50% of the CPF was removed after 9 h given the conditions of the photoreactor setup and TiO₂ concentration (20 mg L⁻¹). CPF can be susceptible to base catalyzed hydrolysis, however no degradation products were observed for any of the dark series (Data in SI4). Additionally, the working stock solutions showed no decrease in concentration with time (Data in SI4).

Degradation of CPF and CPF Oxon and TCP production are shown in Figure 2. Summing the three analytes returns an acceptable mole balance (90.8-105.3% recovery), indicating that the formation of additional primary degradation products is unlikely. After 24 h of continual UV exposure, 81% of CPF was degraded, and the rate of CPF Oxon formation slowed, though a decrease in CPF Oxon concentration was not observed over the sampling period.

Figure 2- CPF degradation and degradation product concentration versus time exposed 20 mg L⁻¹ TiO₂ and UV. UV irradiance at the suspension surface was 2.0 mW cm⁻².

Data were fit using the CAKE software package and followed first order reaction kinetics (Data in SI). The half-life ($t_{1/2}$) of CPF was calculated to be 443 min under the given conditions, while half-lives for CPF Oxon and TCP were calculated to be on the order of hundreds of hours (Figure 2, inset). CPF Oxon is the predominant degradation product produced via oxidation of the sulfur in the phosphorothioate group, and this pathway represents 84% of the calculated CPF Degradation. TCP formation, formed through ester cleavage, makes up the balance at 16%. In agreement with the mole balance achieved, no significant loss of CPF to an unidentified sink was identified, though this pathway was included as an option as illustrated in Figure 3. The further oxidation of CPF Oxon to TCP was not quantifiable, most likely due to reactor conditions resulting in little CPF Oxon degradation over 24 h.

Figure 3 – Potential degradation pathways considered by Cake software

3.4. Bacterial Impact of UV/TiO₂ exposure

The hydroxyl radical is primarily responsible for bacterial inactivation as determined through the use of ROS quenchers (Data in SI2). Strong inactivation was observed for both *B. subtilis* and *A. baumannii* when exposed to UV irradiated TiO₂. *B. subtilis* was completely inactivated over 60 minutes of irradiation (Figure 4, grey squares), while for *A. baumannii*, fewer than 10% of CFU remained after 60 minutes (Figure SI-5). The addition of SOD did not alter the inactivation rate of either *A. baumannii* or *B. subtilis*, indicating superoxide was not generated at sufficient concentrations to contribute to bacteria toxicity. Conversely, no inactivation was observed when bacteria were irradiated in a TiO₂ suspension to which the •OH quencher N-AC was added, further implicating •OH as the primary active agent (Figure 4, black triangles).

Figure 4 – Inactivation of B. subtilis under the following conditions: 20 mg L⁻¹ TiO₂ exposed to UV (UV+), 20 mg L⁻¹ TiO₂ exposed to UV in the presence of SOD (SOD), 20 mg L⁻¹ TiO₂ exposed to UV in the presence of N-AC (N-AC), 20 mg L⁻¹ TiO₂ under dark conditions (D+), and 0 mg L⁻¹ TiO₂ exposed to UV (UV-). UV irradiance at the suspension surface was 2.3 mW cm⁻².

TEM of bacteria exposed to UV light both in the presence and absence of NPs for 60 min show small clusters of nanoparticles observed in close proximity to ruptured segments of cell membranes (Figure 5a, b). These images further support the evidence indicating that locally generated reactive oxygen species are responsible for loss of membrane integrity and cell death, and agree with previous studies [53-55].

Figure 5 – TEM images of B. subtilis with 20 mg L⁻¹ TiO₂ a) prior to UV exposure and b) after 60min UV exposure. Scale bars are 500nm.

3.5. Bacterial Impact of CPF and degradation products exposure

To investigate if the sorption of an organic contaminant affects bacterial inactivation (either positively or negatively), bacteria were irradiated in the UV/TiO₂ system in the presence of CPF at 375 µg L⁻¹. Inactivation was measured after allowing CPF to sorb to the mineral surface for 60 minutes in the dark and compared to inactivation from TiO₂ not exposed to CPF. The presence of CPF did not produce a significant difference in inactivation from suspensions without CPF, as shown in Figure SI-6. Additionally, no inactivation was observed following incubation of bacteria for up to 1 h in the resulting combination of CPF, TiO₂ nanoparticles, and CPF degradation products created by 60 min of UV irradiation. Furthermore, CPF by itself did not inactivate *A. baumannii* or *B. subtilis* over 60 min of exposure. Finally, CPF Oxon, and TCP, the primary degradation products, were dosed at the equivalent molar concentrations used for CPF to simulate complete transformation of the pesticide to a degradation product. Neither CPF Oxon nor TCP was found to be acutely toxic to either *A. baumannii* or *B. subtilis* (Figure SI-8).

3.6. Impact of Bacteria and CPF on TiO₂ Reactivity

To determine the impact that the presence of additional constituents in suspension had on reactivity, •OH production was measured in both the presence and absence of CPF and *B. subtilis*. CPF was added to a TiO₂ suspension and mixed briefly in the dark prior to the addition of TA and exposure to UV-A for 5 min. The resulting suspensions contained 1.098 µM CPF and 125 µM TA. 2-HTA fluorescence represents the amount of hydroxyl radicals that are detected in the bulk. As can be seen in Table 1a, the presence of CPF decreased the amount of hydroxyl radicals detected by TA by 88±1.3%. No change in reactivity was observed compared to initial values when CPF and TiO₂ were mixed up to 60 min before the addition of TA and illumination (Table 1b). This is consistent with the lack of sorption observed in section 3.2. Furthermore, time resolved DLS did not indicate TiO₂ aggregation in the presence of CPF (Figure SI-3).

Similarly, *B. subtilis* was added to a suspension of TiO₂ at a concentration of 10⁸ cfu ml⁻¹ and reactivity was subsequently measured via TA. The presence of bacteria decreased 2-HTA fluorescence by 56±10%. When both CPF and *B. subtilis* are present in suspension, fluorescence decreased by 94±0.4%. This value is greater than dark controls (96±0.8%), indicating that a small amount of hydroxyl radicals are still detected by the probe compound.

3.7. Impact of Bacteria on CPF degradation

CPF degradation tests were performed in the presence of *B. subtilis* at 20 mg L⁻¹ TiO₂. Given the reactivity measurements observed in section 3.6, it was expected that TiO₂ association with the bacteria would reduce the degradation rate of CPF. However, no difference was seen in CPF loss rates with bacteria compared to without ($p > 0.05$) (Figure 6). Dark controls indicated negligible CPF Oxon or TCP production, and 92-115% recovery over 24 h. (Figure SI-4).

Figure 6 – Degradation of CPF in the presence and absence of bacteria. UV irradiance at the suspension surface was 2.0 mW cm⁻².

4. Discussion

4.1. TiO₂ Photocatalysis

Photodegradation rates depend upon many factors (e.g. UV flux, contaminant concentration, and photocatalyst loading) making direct comparisons of studies difficult. In this work, reactor conditions were selected to better observe the interactions between TiO₂, CPF, and bacteria. The concentration of CPF used in this study (375 µg L⁻¹) was selected due to the low aqueous solubility of the pesticide. However there is great variability reported in the literature for CPF solubility, Solubility values as low as 300 µg L⁻¹ have been reported, although Gebremariam et al. report an average of 600±330 µg L⁻¹ in distilled water [4]. Frequently, degradation studies have far exceeded this solubility, with concentrations ranging from mg L⁻¹ to hundreds of mg L⁻¹, often by using significant concentrations of co-solvents [29, 30, 56, 57]. By selecting a lower concentration of the pesticide, we minimize unexplained losses arising from the compound's hydrophobicity.

In addition to large CPF concentrations, degradation studies have often employed high catalyst loading with the goal of maximizing the photodegradation rate [27]. Generally, ROS production is seen to improve with increasing TiO₂ concentration up to the point when light penetration becomes the limiting factor in photoexcitation. The concentration at which this optimal production occurs varies widely depending on experimental setup, with optimum TiO₂ concentrations in the low g L⁻¹ range being reported [30, 58]. Even at the lower end, nanoparticle particle concentrations frequently employed are an order of magnitude greater than the 20 mg L⁻¹ applied in the current study. Using a lower catalyst loading effectively prolongs the degradation process, allowing better insight into the potential pathways of CPF removal from solution. For comparison, whereas $t_{1/2}$ for CPF in this study was 443 min, Kanmoni et al, using a 10x greater catalyst loading (250 mg L⁻¹) achieved half lives of 25 min using solar radiation [56]. Similarly, Devi et al. observed $t_{1/2}$ of 22 min for CPF using 600 mg L⁻¹ TiO₂ [59].

4.2. CPF Adsorption

While high affinity of CPF for soil particulate matter has often been observed [5, 31, 60], generally, few attempts have been made to identify sorption versus degradation of CPF using TiO₂. Devi et al. report an 8% loss of CPF from suspension after mixing in the presence of

150 mg anatase for 10 min in the dark, which is ascribed to adsorption [59]. It is unclear, however what concentrations of CPF were used in this study, and an attempt to extract the pesticide off of the TiO_2 to validate the proposed does not appear to have been made.

Studies focusing on the interactions and surface catalyzed hydrolysis of chlorpyrifos methyl and other related pesticides using metal oxides have generally found little to no sorption. Nair et al., looking at adsorption of CPF onto Al_2O_3 found complete removal of the pesticide when the mineral surface was coated with Au and Ag NPs, but that no significant adsorption occurred with bare Al_2O_3 spheres [31]. Furthermore, Torrents et al. observed the slow loss of chlorpyrifos methyl from solution in a 10 g L^{-1} TiO_2 suspension, but concluded this decrease was likely due to hydrolysis rather than sorption [32]. The rate of hydrolysis by TiO_2 was greater than that for equivalent concentrations of Al_2O_3 or FeOOH . Clausen and Fabricius, utilizing α - and γ - FeOOH , showed that absorption, while significant for ionic pesticides, was negligible for nonionic pesticides [33].

These studies support our current observations for the nonionic chlorpyrifos, and suggest that the use of TiO_2 NPs alone will not contribute practically to CPF adsorptive removal from solution in a remediation scenario. As a result, loss of CPF is likely to occur almost entirely through photocatalysis. The timeline for TiO_2 surface catalyzed hydrolysis presented by Torrents et al. indicate that the order of days is necessary for tens of g L^{-1} of NPs to degrade CPF appreciably, while this study, using a thousand-fold less TiO_2 , is capable of achieving a 50% reduction in CPF in 9 h [32]. Furthermore, the lack of specific interactions implies that other components of natural waters, such as bacteria or NOM, which may show a stronger affinity for TiO_2 , are likely to further limit access to the TiO_2 surface.

4.3. CPF Degradation and Oxidation Products

Many Duirk et al. observed both CPF Oxon and TCP formation from oxidation of CPF using HOCl as the oxidant [61]. The relative amounts of the degradation products produced are in good agreement with the current study, in which the fraction of CPF transformed via oxidation of the sulfur, far exceeds cleavage of the ester bond to create TCP. Devi et al. present a similar pathway [59]. Thus, while ester cleavage may be the predominant pathway for surface catalyzed hydrolysis, oxidation produces an intermediary, which is then capable of forming TCP or further degrading via an alternative pathway.

4.4. TiO_2 Reactivity in Mixed Systems

The formation of ROS occurs at the surface of the TiO_2 nanoparticle, which then diffuses away from the surface into the bulk solution, nonspecifically reacting with targets it comes across [62]. As each compound in solution competes for a fraction of the finite amount of ROS generated, delivery depends not only on individual reaction rates but also on proximity to the NP surface. Because $\bullet\text{OH}$ generated by heterogeneous photocatalysis is produced at a specific point (versus homogenous photocatalysis, e.g., hydrogen peroxide which is uniformly mixed in aqueous solutions) the closer a target is to the photocatalyst, the greater the subsequent radical dose. The use of a probe compound such as TA is capable of providing a benchmark of the $\bullet\text{OH}$ concentration in the bulk solution. In this study, increasing the complexity of the water chemistry reduces the bulk $\bullet\text{OH}$ detected in the system.

When CPF is introduced into the system, TA fluorescence strongly decreases, suggesting that the majority of $\bullet\text{OH}$ are delivered to other targets in the water. The $\bullet\text{OH}$ reacts with TA and CPF at roughly equal rate of $3.3 \times 10^9 \text{ M}^{-1} \text{ s}^{-1}$ and $4.4 \times 10^9 \text{ M}^{-1} \text{ s}^{-1}$, respectively [63, 64]. Given that the concentration of CPF present in solution ($1.098 \text{ } \mu\text{M}$) was two orders of magnitude less than that of TA ($125 \text{ } \mu\text{M}$), one would expect the presence of CPF to have a negligible impact in 2-HTA formation, and thus fluorescence. As a result, the reduction in TA fluorescence can be partially attributed to the presence of methanol necessary to suspend CPF in the system ($k = 7.5 \times 10^8 \text{ M}^{-1} \text{ s}^{-1}$) [65]. Despite this additional sink of $\bullet\text{OH}$, no change in bacterial inactivation is observed in the mixed system.

Conversely, nor does the presence of bacteria impact CPF degradation over 24 h. This implies that, despite TiO_2 affinity for the bacterial surface, there remains sufficient $\bullet\text{OH}$ production for CPF degradation to continue unaffected. These data are in contrast to the reduction in detected $\bullet\text{OH}$ by TA in the presence of *B. subtilis* (Section 3.6) and suggest that differences in relative affinity for the NP act as significant deciders of delivered ROS dose.

Though sorption of CPF onto the surface of TiO_2 is not observed (Section 3.2), relatively weaker hydrophobic interactions are likely to draw the nonionic CPF towards the NP surface. Additionally, the two partially positive ethyl functional groups attached to the more electronegative phosphorothioate in CPF will produce a small dipole moment that may encourage interaction with the negatively charged NP surface. These ion-dipole interactions are likely to be smaller in magnitude compared to ion-ion repulsive forces between TiO_2 and the negatively charged carboxylic groups on TA (pK_a 3.5, 4.5) [64], but the effect will be the same in either case. These electrostatic interactions, coupled with the hydrophobic interactions of CPF, will draw CPF molecules closer to the surface of the negatively charged TiO_2 and increase exposure to generated $\bullet\text{OH}$.

The nature of these interactions between CPF and the NP surface, however, is not so strong that it displaces bacteria or alters the rate of inactivation, as observed in Figure SI-6. These data, coupled with TEM images in which NPs are observed at the surface of bacteria both prior to and following UV exposure, indicate that NPs attach to the cell providing a direct pathway for $\bullet\text{OH}$ delivery. These results imply that the CPF remediation process itself (i.e. photoactivated TiO_2) will likely have a greater impact on microbial viability than either the pesticide or its degradation products at concentrations below the solubility limit given the lack of acute toxicity observed.

5. Conclusions

This work has investigated the photoreactivity of titanium dioxide nanoparticles, the capability to degrade the pesticide chlorpyrifos, and the effect of and impact on bacteria during the photodegradation process. Photocatalytic degradation of CPF produced both chlorpyrifos oxon and 3,5,6-trichloro-2-pyridinol, with 80% degradation of CPF achieved after 24h in our reactor, irrespective of the presence of bacteria. Bacterial inactivation was comparatively rapid, with complete inactivation of *B. subtilis* observed after 60 minutes. The presence of CPF did not change inactivation rates, although the presence of *B. subtilis* reduced bulk $\bullet\text{OH}$ detection by 56%. In the presence of both bacteria and CPF, detected bulk $\bullet\text{OH}$ was reduced by up to 94%. Thus, the picture that emerges from the given study that the

components of an aqueous system are impacted relative to their affinity for the TiO₂ NPs. Arising from this is the implication that while investigating reactivity in simplified systems can provide a benchmark of NP reactivity, it may also overestimate photocatalytic efficiency in realistic environments, especially for hydrophilic contaminants, and that more research in complex systems and natural waters should be undertaken to better understand the role that non-targeted entities may play in remediation scenarios.

Acknowledgements

Funding for this work was gratefully provided by the NIEHS-supported Duke University Superfund Research Center (NIEHS grant P42-ES010356). Additionally, this material is based upon work supported by the National Science Foundation (GRFP DGF1106401). The authors also thank Dr. Niall O'Brien for his fruitful discussions.

References

- [1] L.E. Gomez, Use and benefits of chlorpyrifos in US agriculture, Dow AgroSciences LLC, (2009).
- [2] Z. Chishti, S. Hussain, K.R. Arshad, A. Khalid, M. Arshad, Microbial degradation of chlorpyrifos in liquid media and soil, *Journal of environmental management*, 114 (2013) 372-380.
- [3] S. Armenta, G. Quintás, S. Garrigues, M. de la Guardia, A validated and fast procedure for FTIR determination of Cypermethrin and Chlorpyrifos, *Talanta*, 67 (2005) 634-639.
- [4] S.Y. Gebremariam, M.W. Beutel, D.R. Yonge, M. Flury, J.B. Harsh, Adsorption and Desorption of Chlorpyrifos to Soils and Sediments, *Rev Environ Contam T*, 215 (2012) 123-175.
- [5] S. Baskaran, R.S. Kookana, R. Naidu, Contrasting behaviour of chlorpyrifos and its primary metabolite, TCP (3,5,6-trichloro-2-pyridinol), with depth in soil profiles, *Aust J Soil Res*, 41 (2003) 749-760.
- [6] R.J. Gilliom, J.E. Barbash, C.G. Crawford, P.A. Hamilton, J.D. Martin, N. Nakagaki, L.H. Nowell, J.C. Scott, P.E. Stackelberg, G.P. Thelin, *Pesticides in the nation's streams and ground water, 1992-2001*, Geological Survey (US), 2006.
- [7] E. Estevez, M. del Carmen Cabrera, J.R. Fernández-Vera, A. Molina-Díaz, J. Robles-Molina, M. del Pino Palacios-Díaz, Monitoring priority substances, other organic contaminants and heavy metals in a volcanic aquifer from different sources and hydrological processes, *Sci Total Environ*, 551 (2016) 186-196.
- [8] M.P. Ensminger, R. Budd, K.C. Kelley, K.S. Goh, Pesticide occurrence and aquatic benchmark exceedances in urban surface waters and sediments in three urban areas of California, USA, 2008–2011, *Environmental monitoring and assessment*, 185 (2013) 3697-3710.
- [9] A.W. Jarvinen, B.R. Nordling, M.E. Henry, Chronic toxicity of Dursban (chlorpyrifos) to the fathead minnow (*Pimephales promelas*) and the resultant acetylcholinesterase inhibition, *Ecotoxicology and environmental safety*, 7 (1983) 423-434.
- [10] J.P. Giesy, K.R. Solomon, J.R. Coats, K.R. Dixon, J.M. Giddings, E.E. Kenaga, *Chlorpyrifos: ecological risk assessment in North American aquatic environments*, Springer, 1999.

- [11] D.L. Eaton, R.B. Daroff, H. Autrup, J. Bridges, P. Buffler, L.G. Costa, J. Coyle, G. McKhann, W.C. Mobley, L. Nadel, D. Neubert, R. Schulte-Hermann, P.S. Spencer, Review of the toxicology of chlorpyrifos with an emphasis on human exposure and neurodevelopment, *Critical reviews in toxicology*, 38 Suppl 2 (2008) 1-125.
- [12] J. Risher, H.A. Navarro, Toxicological profile for chlorpyrifos, US Department of Health and Human Services, Atlanta, (1997).
- [13] D. Qiao, F.J. Seidler, T.A. Slotkin, Developmental neurotoxicity of chlorpyrifos modeled in vitro: Comparative effects of metabolites and other cholinesterase inhibitors on DNA synthesis in PC12 and C6 cells, *Environ Health Persp*, 109 (2001) 909-913.
- [14] K.D. Racke, D.D. Fontaine, R.N. Yoder, J.R. Miller, Chlorpyrifos degradation in soil at termiticidal application rates, *Pestic Sci*, 42 (1994) 43-51.
- [15] S. Baskaran, R.S. Kookana, R. Naidu, Degradation of bifenthrin, chlorpyrifos and imidacloprid in soil and bedding materials at termiticidal application rates, *Pestic Sci*, 55 (1999) 1222-1228.
- [16] E.M. John, J.M. Shaike, Chlorpyrifos: pollution and remediation, *Environmental Chemistry Letters*, 13 (2015) 269-291.
- [17] J.M. Smolen, A.T. Stone, Metal (hydr)oxide surface catalyzed hydrolysis of chlorpyrifos-methyl, chlorpyrifos-methyl oxon, and paraoxon, *Soil Sci Soc Am J*, 62 (1998) 636-643.
- [18] M.T. Rose, A.N. Crossan, I.R. Kennedy, Dissipation of cotton pesticides from runoff water in glasshouse columns, *Water, air, and soil pollution*, 182 (2007) 207-218.
- [19] K.R. Solomon, W.M. Williams, D. Mackay, J. Purdy, J.M. Giddings, J.P. Giesy, Properties and uses of chlorpyrifos in the United States, *Reviews of environmental contamination and toxicology*, 231 (2014) 13-34.
- [20] M.R. Hoffmann, S.T. Martin, W.Y. Choi, D.W. Bahnemann, Environmental Applications of Semiconductor Photocatalysis, *Chem Rev*, 95 (1995) 69-96.
- [21] M.N. Chong, B. Jin, C.W. Chow, C. Saint, Recent developments in photocatalytic water treatment technology: a review, *Water Res*, 44 (2010) 2997-3027.
- [22] D.S. Bhatkhande, V.G. Pangarkar, A.A.C.M. Beenackers, Photocatalytic degradation for environmental applications - a review, *Journal of Chemical Technology & Biotechnology*, 77 (2002) 102-116.
- [23] U.I. Gaya, A.H. Abdullah, Heterogeneous photocatalytic degradation of organic contaminants over titanium dioxide: A review of fundamentals, progress and problems, *Journal of Photochemistry and Photobiology C: Photochemistry Reviews*, 9 (2008) 1-12.
- [24] C. McCullagh, N. Skillen, M. Adams, P.K.J. Robertson, Photocatalytic reactors for environmental remediation: a review, *Journal of Chemical Technology & Biotechnology*, 86 (2011) 1002-1017.
- [25] M.M. Khin, A.S. Nair, V.J. Babu, R. Murugan, S. Ramakrishna, A review on nanomaterials for environmental remediation, *Energy & Environmental Science*, 5 (2012) 8075.
- [26] S. Kwon, M. Fan, A.T. Cooper, H. Yang, Photocatalytic Applications of Micro- and Nano-TiO₂ in Environmental Engineering, *Critical Reviews in Environmental Science and Technology*, 38 (2008) 197-226.
- [27] A. Dârjan, C. Drăghici, D. Perniu, A. Duță, Degradation of Pesticides by TiO₂ Photocatalysis, (2013) 155-163.

- [28] T. Ochiai, A. Fujishima, Photoelectrochemical properties of TiO₂ photocatalyst and its applications for environmental purification, *Journal of Photochemistry and Photobiology C: Photochemistry Reviews*, 13 (2012) 247-262.
- [29] A.C. Affam, M. Chaudhuri, Degradation of pesticides chlorpyrifos, cypermethrin and chlorothalonil in aqueous solution by TiO₂ photocatalysis, *Journal of environmental management*, 130 (2013) 160-165.
- [30] A. Fadaei, M. Kargar, Photocatalytic degradation of chlorpyrifos in water using titanium dioxide and zinc oxide, *Fresenius Environmental Bulletin*, 22 (2013) 2442-2447.
- [31] A.S. Nair, T. Pradeep, Extraction of chlorpyrifos and malathion from water by metal nanoparticles, *J Nanosci Nanotechnol*, 7 (2007) 1871-1877.
- [32] A. Torrents, A.T. Stone, Oxide surface-catalyzed hydrolysis of carboxylate esters and phosphorothioate esters, *Soil Sci Soc Am J*, 58 (1994) 738-745.
- [33] L. Clausen, I. Fabricius, Atrazine, isoproturon, mecoprop, 2, 4-D, and bentazone adsorption onto iron oxides, *J Environ Qual*, 30 (2001) 858-869.
- [34] T. Hofmann, F. von der Kammer, Estimating the relevance of engineered carbonaceous nanoparticle facilitated transport of hydrophobic organic contaminants in porous media, *Environmental pollution*, 157 (2009) 1117-1126.
- [35] M.N. Moore, Do nanoparticles present ecotoxicological risks for the health of the aquatic environment?, *Environ Int*, 32 (2006) 967-976.
- [36] L. Wang, Y. Huang, A.T. Kan, M.B. Tomson, W. Chen, Enhanced transport of 2,2',5,5'-polychlorinated biphenyl by natural organic matter (NOM) and surfactant-modified fullerene nanoparticles (nC₆₀), *Environ Sci Technol*, 46 (2012) 5422-5429.
- [37] N. Pino, G. Peñuela, Simultaneous degradation of the pesticides methyl parathion and chlorpyrifos by an isolated bacterial consortium from a contaminated site, *International Biodeterioration & Biodegradation*, 65 (2011) 827-831.
- [38] B.K. Singh, A. Walker, J.A. Morgan, D.J. Wright, Biodegradation of chlorpyrifos by enterobacter strain B-14 and its use in bioremediation of contaminated soils, *Applied and environmental microbiology*, 70 (2004) 4855-4863.
- [39] B.K. Singh, A. Walker, J.A.W. Morgan, D.J. Wright, Effects of Soil pH on the Biodegradation of Chlorpyrifos and Isolation of a Chlorpyrifos-Degrading Bacterium, *Applied and environmental microbiology*, 69 (2003) 5198-5206.
- [40] J.M. Bifulco, J. Shirey, G. Bissonnette, Detection of *Acinetobacter* spp. in rural drinking water supplies, *Applied and environmental microbiology*, 55 (1989) 2214-2219.
- [41] S. Anwar, F. Liaquat, Q.M. Khan, Z.M. Khalid, S. Iqbal, Biodegradation of chlorpyrifos and its hydrolysis product 3,5,6-trichloro-2-pyridinol by *Bacillus pumilus* strain C2A1, *J Hazard Mater*, 168 (2009) 400-405.
- [42] F. Ahmad, S. Iqbal, S. Anwar, M. Afzal, E. Islam, T. Mustafa, Q.M. Khan, Enhanced remediation of chlorpyrifos from soil using ryegrass (*Lolium multiflorum*) and chlorpyrifos-degrading bacterium *Bacillus pumilus* C2A1, *J Hazard Mater*, 237 (2012) 110-115.
- [43] Y. Ge, J.P. Schimel, P.A. Holden, Evidence for negative effects of TiO₂ and ZnO nanoparticles on soil bacterial communities, *Environ Sci Technol*, 45 (2011) 1659-1664.
- [44] G. Imfeld, S. Vuilleumier, Measuring the effects of pesticides on bacterial communities in soil: A critical review, *European Journal of Soil Biology*, 49 (2012) 22-30.
- [45] P. Palma, V.L. Palma, R.M. Fernandes, A.M. Soares, I.R. Barbosa, Acute toxicity of atrazine, endosulfan sulphate and chlorpyrifos to *Vibrio fischeri*, *Thamnocephalus platyurus*

and *Daphnia magna*, relative to their concentrations in surface waters from the Alentejo region of Portugal, *Bull Environ Contam Toxicol*, 81 (2008) 485-489.

[46] T.J. Battin, F.V. Kammer, A. Weilhartner, S. Ottofueiling, T. Hofmann, Nanostructured TiO₂: transport behavior and effects on aquatic microbial communities under environmental conditions, *Environ Sci Technol*, 43 (2009) 8098-8104.

[47] L. Brunet, D.Y. Lyon, E.M. Hotze, P.J.J. Alvarez, M.R. Wiesner, Comparative Photoactivity and Antibacterial Properties of C-60 Fullerenes and Titanium Dioxide Nanoparticles, *Environ Sci Technol*, 43 (2009) 4355-4360.

[48] M. Lazar, S. Varghese, S. Nair, Photocatalytic Water Treatment by Titanium Dioxide: Recent Updates, *Catalysts*, 2 (2012) 572-601.

[49] L.K. Adams, D.Y. Lyon, P.J. Alvarez, Comparative eco-toxicity of nanoscale TiO₂, SiO₂, and ZnO water suspensions, *Water Res*, 40 (2006) 3527-3532.

[50] M. Biguzzi, G. Shama, Effect of titanium dioxide concentration on the survival of *Pseudomonas stutzeri* during irradiation with near ultraviolet light, *Letters in Applied Microbiology*, 19 (1994) 458-460.

[51] D.Y. Lyon, L.K. Adams, J.C. Falkner, P.J.J. Alvarez, Antibacterial activity of fullerene water suspensions: Effects of preparation method and particle size, *Environ Sci Technol*, 40 (2006) 4360-4366.

[52] J. Taurozzi, V. Hackley, M. Wiesner, Preparation of a nanoscale TiO₂ aqueous dispersion for toxicological or environmental testing, NIST Special Publication, 1200 (2012) 3.

[53] G. Gogniat, M. Thyssen, M. Denis, C. Pulgarin, S. Dukan, The bactericidal effect of TiO₂ photocatalysis involves adsorption onto catalyst and the loss of membrane integrity, *FEMS microbiology letters*, 258 (2006) 18-24.

[54] A.M. Horst, A.C. Neal, R.E. Mielke, P.R. Sislian, W.H. Suh, L. Mädler, G.D. Stucky, P.A. Holden, Dispersion of TiO₂ nanoparticle agglomerates by *Pseudomonas aeruginosa*, *Applied and environmental microbiology*, 76 (2010) 7292-7298.

[55] B. Jalvo, M. Faraldos, A. Bahamonde, R. Rosal, Antimicrobial and antibiofilm efficacy of self-cleaning surfaces functionalized by TiO₂ photocatalytic nanoparticles against *Staphylococcus aureus* and *Pseudomonas putida*, *J Hazard Mater*, 340 (2017) 160-170.

[56] V.G.G. Kanmoni, S. Daniel, G.A.G. Raj, Photocatalytic degradation of chlorpyrifos in aqueous suspensions using nanocrystals of ZnO and TiO₂, *Reaction Kinetics, Mechanisms and Catalysis*, 106 (2012) 325-339.

[57] K. Sivagami, R.R. Krishna, T. Swaminathan, Photo Catalytic Degradation of Chlorpyrifos in an Annular Slurry Reactor, *Journal of Water Sustainability*, 3 (2013) 143-151.

[58] A. Verma, D. Dixit, Photocatalytic degradability of insecticide Chlorpyrifos over UV irradiated Titanium dioxide in aqueous phase, *International Journal of Environmental Sciences*, 3 (2012) 743-755.

[59] L.G. Devi, B.N. Murthy, S.G. Kumar, Photocatalytic activity of V⁵⁺, Mo⁶⁺ and Th⁴⁺ doped polycrystalline TiO₂ for the degradation of chlorpyrifos under UV/solar light, *Journal of Molecular Catalysis A: Chemical*, 308 (2009) 174-181.

[60] M.J. Redondo, M.J. Ruiz, G. Font, R. Boluda, Dissipation and distribution of atrazine, simazine, chlorpyrifos, and tetradifon residues in citrus orchard soil, *Arch Environ Con Tox*, 32 (1997) 346-352.

- [61] S.E. Duirk, T.W. Collette, Degradation of chlorpyrifos in aqueous chlorine solutions: Pathways, kinetics, and modeling, *Environ Sci Technol*, 40 (2006) 546-551.
- [62] A.L. Linsebigler, G.Q. Lu, J.T. Yates, Photocatalysis on TiO_2 Surfaces - Principles, Mechanisms, and Selected Results, *Chem Rev*, 95 (1995) 735-758.
- [63] K.L. Armbrust, Pesticide hydroxyl radical rate constants: measurements and estimates of their importance in aquatic environments, *Environ Toxicol Chem*, 19 (2000) 2175-2180.
- [64] S.E. Page, W.A. Arnold, K. McNeill, Terephthalate as a probe for photochemically generated hydroxyl radical, *Journal of environmental monitoring : JEM*, 12 (2010) 1658-1665.
- [65] G.V. Buxton, C.L. Greenstock, W.P. Helman, A.B. Ross, Critical-Review of Rate Constants for Reactions of Hydrated Electrons, Hydrogen-Atoms and Hydroxyl Radicals ($\text{OH}/\text{O}\cdot$) in Aqueous-Solution, *J Phys Chem Ref Data*, 17 (1988) 513-886.

Figure Captions:

Figure 1 - Supernatant CPF concentrations versus time as a function of TiO_2 concentration (0, 20, 40ppm dark and 20ppm UV). UV irradiance at the suspension surface was 2.0 mW cm^{-2} .

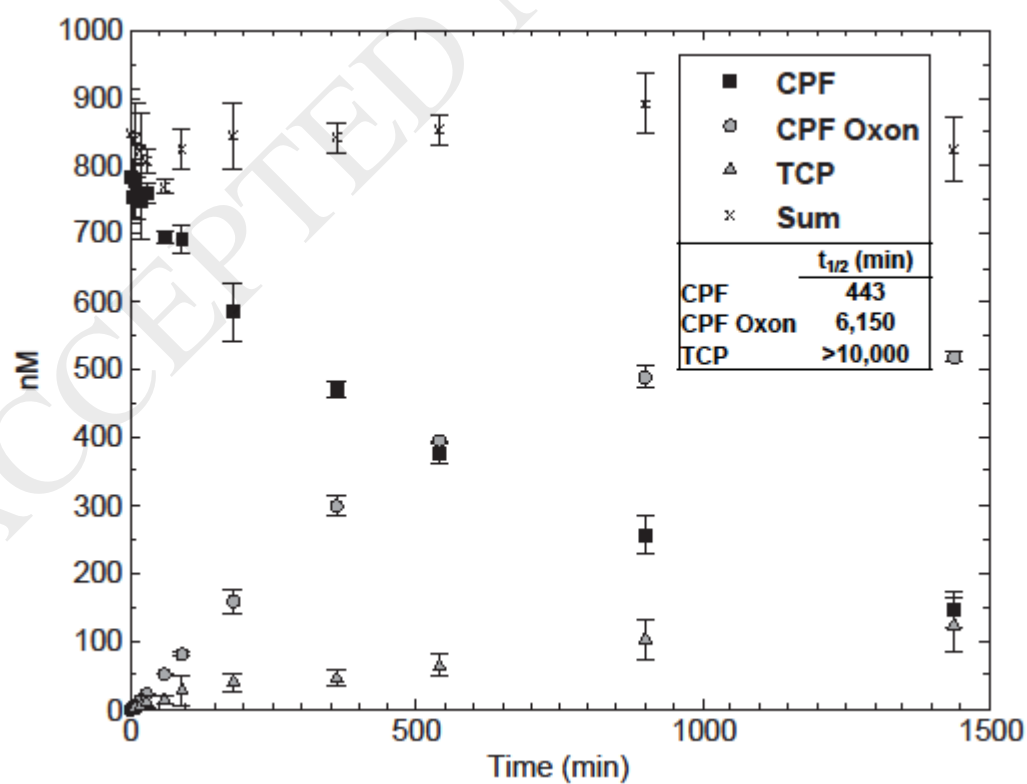
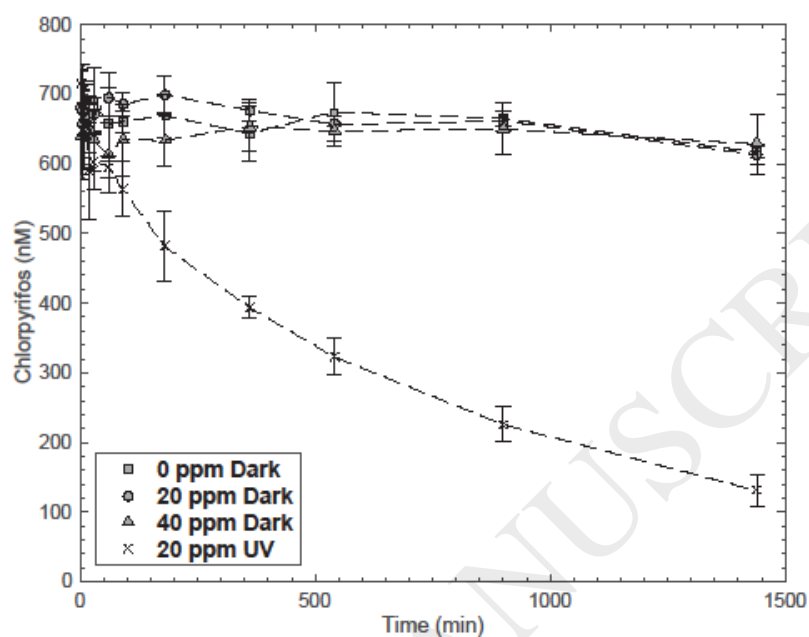
Figure 2- CPF degradation and degradation product concentration versus time exposed $20 \text{ mg L}^{-1} \text{ TiO}_2$ and UV. UV irradiance at the suspension surface was 2.0 mW cm^{-2} .

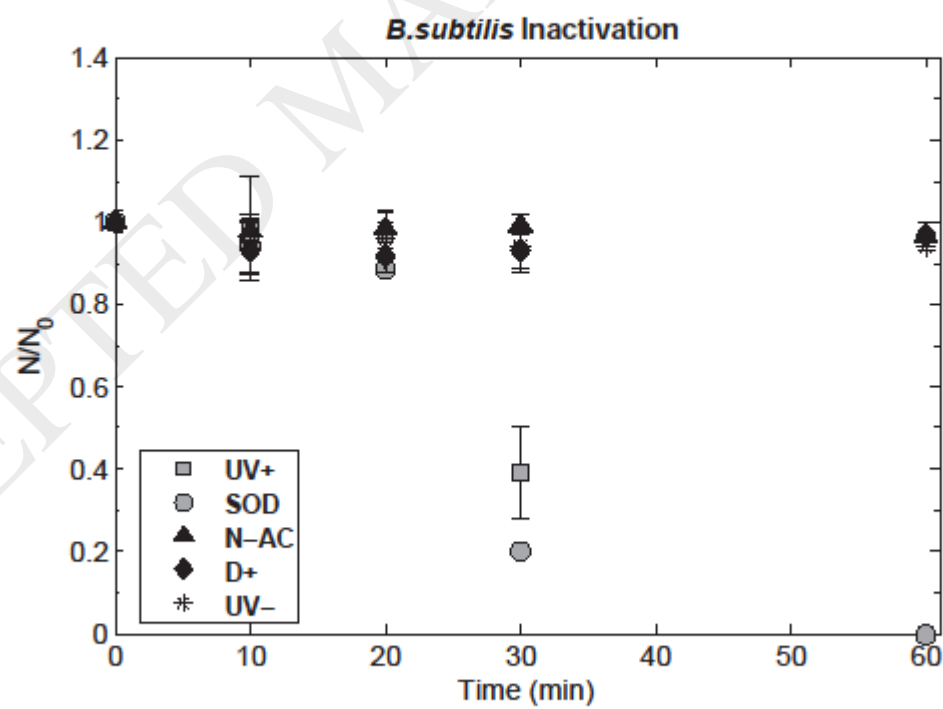
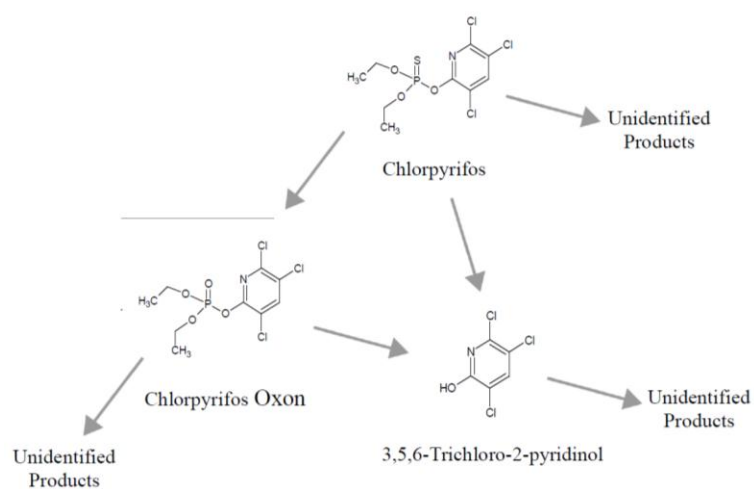
Figure 3 – Potential degradation pathways considered by Cake software.

Figure 4 – Inactivation of *B. subtilis* under the following conditions: $20 \text{ mg L}^{-1} \text{ TiO}_2$ exposed to UV (UV+), $20 \text{ mg L}^{-1} \text{ TiO}_2$ exposed to UV in the presence of SOD (SOD), $20 \text{ mg L}^{-1} \text{ TiO}_2$ exposed to UV in the presence of N-AC (N-AC), $20 \text{ mg L}^{-1} \text{ TiO}_2$ under dark conditions (D+), and $0 \text{ mg L}^{-1} \text{ TiO}_2$ exposed to UV (UV-). UV irradiance at the suspension surface was 2.3 mW cm^{-2} .

Figure 5 – TEM images of *B. subtilis* with 20ppm TiO_2 a) prior to UV exposure and b) after 60min UV exposure. Scale bars are 500nm.

Figure 6 –Degradation of CPF in the presence and absence of bacteria. UV irradiance at the suspension surface was 2.0 mW cm^{-2} .





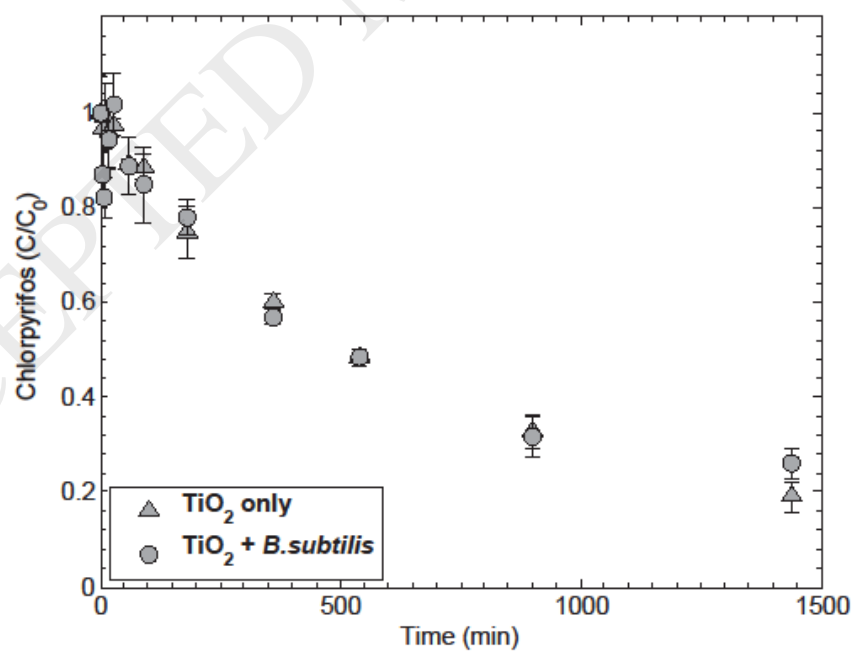
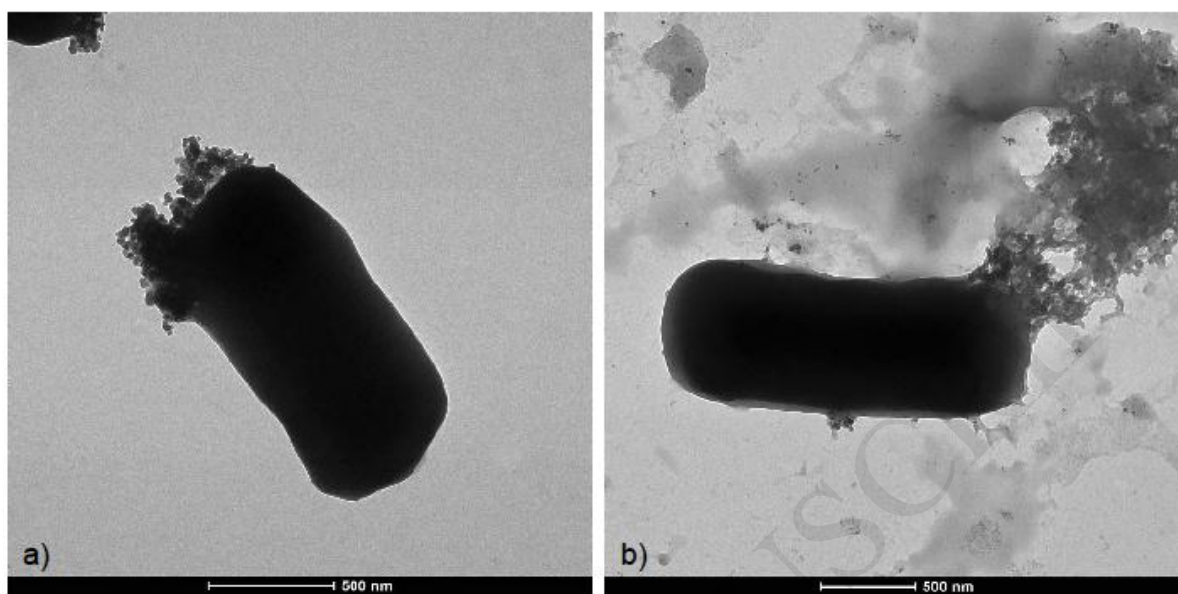


Table 1 –Reactivity measurements of 20 mg L⁻¹ TiO₂ exposed to UV a) Detected •OH from for

various constituents b) Detected $O_2^{\bullet-}$ and $\bullet OH$ in the presence of CPF over 60 minutes.

	Relative Fluorescence	
a) Suspension	Hydroxyl Radical	Superoxide
UV	1.000 ± 0.128	-
<i>B. subtilis</i>	0.439 ± 0.104	-
CPF	0.121 ± 0.013	-
CPF + <i>B. subtilis</i>	0.060 ± 0.004	-
Dark	0.038 ± 0.008	-
b) Time (min)	Hydroxyl Radical	Superoxide
0	1.000 ± 0.109	1.000 ± 0.093
30	1.005 ± 0.137	0.963 ± 0.157
60	0.901 ± 0.100	0.883 ± 0.033